Influence of the Flexibility of Nickel PCP-Pincer Complexes on C–H and P–C Bond Activation and Ethylene Reactivity: A Combined Experimental and Theoretical Investigation

Fengkai He, Christophe Gourlaouen, Huan Pang, Pierre Braunstein

Chemistry Europe
European Chemical Societies Publishing

WILEY VCH

Excellence in Chemistry Research

Announcing our new flagship journal

- Gold Open Access
- Publishing charges waived
- Preprints welcome
- Edited by active scientists

Meet the Editors of *ChemistryEurope*

Luisa De Cola
Università degli Studi di Milano Statale, Italy

Ive Hermans
University of Wisconsin-Madison, USA

Ken Tanaka
Tokyo Institute of Technology, Japan

Chemistry–A European Journal
Research Article
doi.org/10.1002/chem.202104234
Chemistry Europe
European Chemical Societies Publishing
www.chemeurj.org

Influence of the Flexibility of Nickel PCP-Pincer Complexes on C–H and P–C Bond Activation and Ethylene Reactivity: A Combined Experimental and Theoretical Investigation

Fengkai He,[a, b] Christophe Gourlaouen,[c] Huan Pang,*[a] and Pierre Braunstein*[b]

Abstract: Using a pincer platform based on a bridgehead NHC donor with functional side arms, the combined effect of increased flexibility in six-membered pyrimidine-type heterocycles compared to the more often studied five-membered imidazole, and rigidity of phosphane side arms was examined. The unique features observed include: 1) the reaction of the azolium C_{sp2}–H bond with $[Ni(cod)_2]$ affording a carbanionic ligand in $[NiCl(PC_{sp3}{}^{H}P)]$ (**8**) rather than a carbene; 2) its transformation into the NHC, hydrido complex $[NiH(PC^{NHC}P)]PF_6$ (**9**) upon halide abstraction; 3) ethylene insertion into the Ni–H bond of the latter and ethyl migration to the N–*C*–N carbon atom of the heterocycle in $[Ni(PC^{Et}P)]PF_6$ (**10**); and 4) an unprecedented C–P bond activation transforming the $P–C^{NHC}–P$ pincer ligand of **8** in a $C–C^{NHC}–P$ pincer and a terminal phosphanido ligand in $[Ni(PPh_2)(CC^{NHC}P)]$ (**15**). The data are supported by nine crystal structure determinations and theoretical calculations provided insights into the mechanisms of these transformations, which are relevant to stoichiometric and catalytic steps of general interest.

Introduction

The spectacular developments witnessed in the last few years in the chemistry of N-heterocyclic carbenes (NHCs) are rooted in a number of reasons, such as scientific curiosity, emergence of new and often unexpected reactivity patterns, enhanced stability of their metal complexes, tunability of their electronic properties, applications in materials and medicinal sciences, and the often improved performances of NHC-derived catalysts, particularly when compared to related phosphane-based systems.[1–18] The general relevance of NHC chemistry was further highlighted in 2018 by a special issue of *Chemical Reviews*.[19] The incorporation of NHCs into multidentate, hybrid ligands provides increased chemical diversity and can lead to particularly robust catalysts.[20–36] Since their inception in the 1970s, pincer-type ligands, defined as any tridentate ligand that binds to a metal centre in a meridional fashion, have become ubiquitous in modern molecular chemistry, largely because of the kinetic and thermodynamic stabilization they confer to their metal complexes. Incorporating NHC donor(s) in pincer-type architectures has rapidly attracted considerable interest and the huge diversity and relatively easy functionalization of pincer ligands facilitates the fine-tuning of their stereoelectronic features and, consequently, of the reactivity and catalytic applications of their metal complexes.[23,26,28,31,37–47]

Nickel has long been associated with a very rich molecular chemistry, in particular because of the greater flexibility and adaptability of its coordination sphere compared to that of analogous palladium or platinum complexes, and the often-unique structural features and catalytic properties of its metal complexes, in part due to the possibility for Ni^{II} to be in a triplet or singlet ground state, depending on its ligand environment.[48–56] Consequently, it is not surprising that the chemistry of nickel complexes with NHC-containing pincer-type ligands is developing very fast, as documented in recent articles and reviews.[4,35,53,57]

The stereoelectronic properties of NHCs can be modulated by the nature of the N-substituents (or wingtip substituents) and of the heterocycle itself by including or not electronic unsaturation, annelation,[22] or by varying its ring size, typically from five to six. In contrast to five-membered ring NHCs, which attract the most attention, expanded ring NHCs are endowed with higher basicity,[58–61] display larger $N–C^{NHC}–N$ angles,[59,62,63] and represent promising platforms for transition metal reactivity and catalysis.[4,64–67] For a meaningful investigation of the consequences of modifying the stereoelectronic properties of various NHC-containing pincer systems coordinated to a given metal ion, one should either keep the bridgehead (central)

[a] *Dr. F. He, Prof. Dr. H. Pang*
School of Chemistry and Chemical Engineering, Yangzhou University
Yangzhou, 225009, Jiangsu (P. R. China)
E-mail: hefengkai1990@sina.cn
huanpangchem@hotmail.com

[b] *Dr. F. He, Prof. Dr. P. Braunstein*
Laboratoire de Chimie de Coordination
Institut de Chimie (UMR 7177 CNRS), Université de Strasbourg
4 rue Blaise Pascal, 67081 Strasbourg (France)
E-mail: braunstein@unistra.fr

[c] *Dr. C. Gourlaouen*
Laboratoire de Chimie Quantique
Institut de Chimie (UMR 7177 CNRS), Université de Strasbourg
4 rue Blaise Pascal, 67081 Strasbourg (France)
E-mail: gourlaouen@unistra.fr

Supporting information for this article is available on the WWW under https://doi.org/10.1002/chem.202104234

donor constant and vary the wingtip functionalities or keep the latter constant and vary the central donor. In the present combined experimental-theoretical study, a NHC donor will always occupy a bridgehead position and we will examine how the flexibility of pincer systems based on a six-membered heterocycle decorated with two phosphane donors can bring about unique features concerning (i) the reactivity of an azolium C_{sp2}–H bond toward Ni^0, (ii) the insertion of ethylene into a Ni–H bond and subsequent ethyl migration to the heterocycle with C_{sp3}–C_{sp3} bond formation and (iii) an unprecedented C–P bond activation at a P–C^{NHC}–P Ni^0 transient pincer complex resulting in the formation of a Ni^{II} complex with a terminal phosphanido ligand and a new C–C^{NHC}–P pincer ligand.

We recently found that when the bis(imine)imidazolium chloride $[C_3H_3N_2\{C(Me)(=NDiPP)\}_2]Cl$ (**1**) (DiPP = 2,6-diisopropylphenyl) was reacted with $[Ni(cod)_2]$, the imidazolium proton C2–H was surprisingly not removed by oxidative-addition to give a NHC donor but instead, reduction of the proligand occurred and the imidazole C2 carbon became sp^3-hybridized in the resulting $N^{imine}C_{sp3}{}^{H}N^{imine}$ Ni^{II} alkyl pincer complex **2** (Scheme 1).[68]

This finding was unexpected since the direct oxidative-addition of an azolium C–H bond to Ni^0 precursors represents a typical atom economical access to Ni^{II} NHC complexes.[4,69,70] Theoretical calculations showed that the rigidity of the two five-membered metallacycles formed by the $N^{imine}C_{sp3}{}^{H}N^{imine}$ pincer ligand was the main reason for the stability of **2** and the destabilization of the corresponding $N^{imine}C^{NHC}N^{imine}$ pincer system.[68] In comparison, Fryzuk and coll. found that the bis(phosphino)imidazolium hexafluorophosphate **3** reacted with $[Ni(cod)_2]$ to give the expected NHC complex **4**, resulting from the oxidative-addition of the imidazolium C2–H bond to Ni^0 (Scheme 2),[70,71] and the formation of a complex analogous to **2** with a C_{sp3}–Ni bond was not observed. However, with the chloride salt of a closely related bis(phosphino)imidazolium (with PPh_2 instead of P*i*Pr_2 donors), Thomas and coll. observed that reaction with Pd^0 or Pt^0 precursors yielded the corresponding $PC_{sp3}{}^{H}P$ M^{II} chloride pincer complexes (M = Pd, Pt).[72]

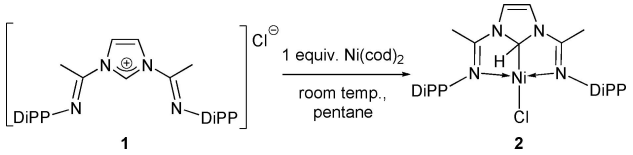

Scheme 1. Synthesis of complex **2** with a $C_{sp3}{}^{H}$–Ni bond.[68]

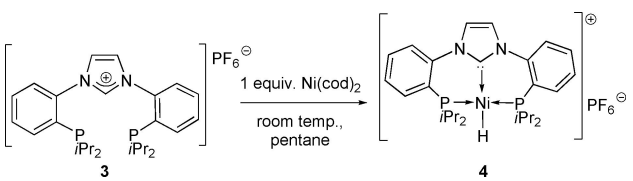

Scheme 2. Synthesis of complex **4** with a C^{NHC}–Ni bond

Chloride abstraction afforded the corresponding cationic hydrido complex with a $PC^{NHC}P$ pincer ligand as a result of H migration from the C_{sp3} to M.

Intrigued by the subtle factors governing the chemoselectivity of such reactions, which are of general relevance to current research performed in numerous groups, we embarked on an experimental and computational study of the impact of increased flexibility in the pincer system on the reactivity of the nickel complexes. Pincer flexibility can be modulated by both the size of the heterocycle containing the bridgehead NHC donor and by the nature of the side arms. With a more flexible six-membered heterocycle, associated with two flexible phosphine donors, the proligand **5** was recently used to readily form pincer complexes of type **6** in which the pincer ligand forms two five-membered metallacycles with Ni^{II} or Pd^{II}, but no intermediate with a carbanionic ligand (C_{sp3}–M bond) was observed in the course of the reaction (Scheme 3).[73] Both the larger ring size of the heterocycle and the CH_2 spacers between P and N provided increased flexibility compared with the situation in **2**.[68]

Results and Discussion

We have now investigated the reactivity of a pincer precursor platform combining a six-membered heterocycle of the hexahydropyrimidinium type, which is more flexible than the five-membered heterocycle in **1**, and relatively rigid phosphane arms, structurally similar to those in **3**, but able to form two six-membered metallacycles more flexible than the five-membered metallacycles in **2**. At this point, the main question was whether the combined effects of the modifications introduced in the functional imidazolium precursor **7** would result in the formation of a 5-electron donor $PC_{sp3}{}^{H}P$ alkyl pincer, as in **2**, or of a 6-electron donor $PC^{NHC}P$-type pincer ligand, as in **4** or **6**.

Gratifyingly, the new bis(phosphino)pyrimidinium salt **7** (see details in the Supporting Information) reacted with 1 equiv. $[Ni(cod)_2]$ in THF at room temperature to afford a neutral complex that displayed a ^1H NMR triplet resonance at δ 3.30, assigned to the NiC–H proton (^3J(P–H) = 16.1 Hz) (Scheme 4). An X-ray diffraction analysis established the tetrahedral environment around the Ni-bound carbon atom in $[NiCl(PC_{sp3}{}^{H}P)]$ (**8**) (Figure 1). The Ni^{II} centre is in a distorted square-planar coordination environment, with two trans phosphane groups and a chloride ligand trans to the sp^3-hybridized carbon (Ni1–C1 1.942(1) Å, C1–Ni1–Cl1 = 157.70(4)°). The heterocycle

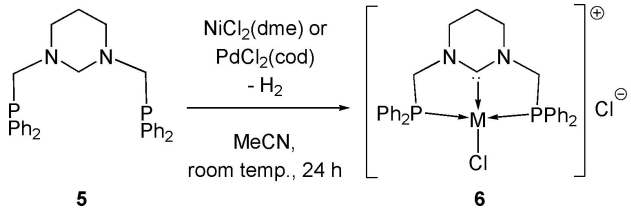

Scheme 3. Synthesis of P–C^{NHC}–P pincer complexes of type **6**.

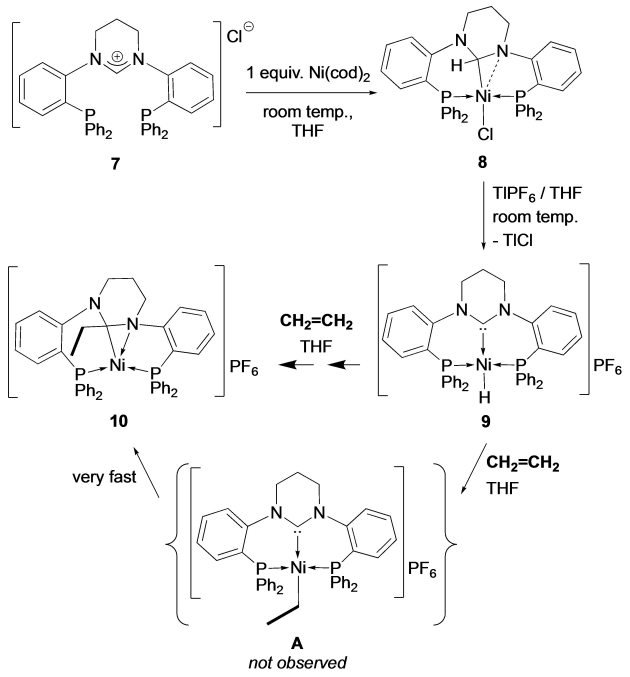

Scheme 4. Formation of the $PC_{sp3}{}^{H}P$ pincer complex **8**, chloride abstraction-promoted H-migration from the C_{sp3} carbon of **8** to Ni in **9**, ethylene insertion into the Ni–H bond and migration of the ethyl ligand from Ni to C^{NHC} to restore a C_{sp3} carbon in **10**. Theoretical calculations did not find any pathway leading to **A** (see below).

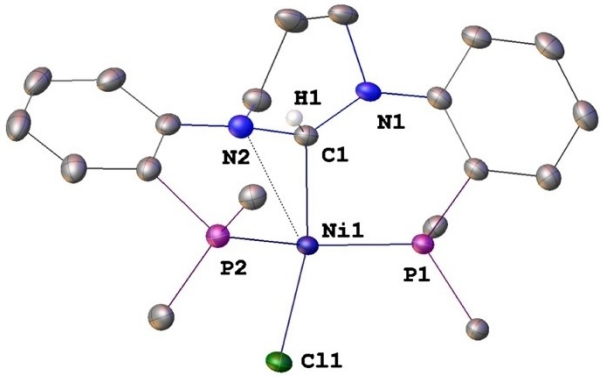

Figure 1. View of the structure of [NiCl($PC_{sp3}{}^{H}P$)] (**8**) in **8**·C_6H_6 with H atoms and benzene molecule omitted for clarity. Only the P-phenyl ipso carbons are shown. Thermal ellipsoids at the 50% probability level. Selected bond lengths (Å) and angles (deg): Ni1–C1 1.942(1), Ni1–Cl1 2.2486(4), Ni1–P1 2.1540(4), Ni1–P2 2.2017(4), Ni1···N2 2.531(1); Ni1–C1–N1 120.23(9), Ni1–C1–N2 95.52(9), C1–Ni1–Cl1 157.70(4), Ni1–C1–H1 110.7, P1–Ni1–P2 154.68(2).

has a distorted envelope-type conformation and is tilted with respect to the Ni–C1 axis (angles (heterocycle centroid)–C1–Ni = 127.8(1)° and (heterocycle centroid)–Ni–Cl = 137.5(1)°), which allows the N2 atom to get much closer to Ni (Ni1···N2 2.531(1) Å) than N1 (2.965(1) Å), thus providing the metal centre with additional electron density. This feature will also be observed in other complexes with the $PC_{sp3}{}^{H}P$ pincer ligand (see below).

The lack of activation of the azolium proton by Ni^0 is again remarkable since Ni^0 is highly competent for such C–H oxidative addition reactions and we are aware of only two precedents.[64,68] The contrast between the isolation of **8** and the formation of **4** (five-membered ring NHC but phosphane donors similar to those in **8**) or **6** (similar 6-membered ring NHC but more flexible donor phosphane arms) nicely illustrates the major impact of subtle modifications in pincer ligand flexibility.

Interestingly, the reaction of **8** with $TlPF_6$ in THF afforded a new complex, **9**, characterized by a ^{1}H NMR resonance at δ −11.79 (t, ^2J(H–P) = 50.0 Hz), typical for a hydrido Ni complex (Scheme 4). No signal corresponding to a NC_{sp3}-H proton was detected. This NHC complex was unambiguously identified by analytical, spectroscopic methods and X-ray diffraction as [NiH($PC^{NHC}P$)]PF_6 (**9**) (Figures 2 and S23). The Ni–C1 distance of 1.899(13) Å is in the range of Ni–carbene bonds and, as expected, is shorter than the Ni-alkyl bond in **8** (1.942(1) Å). The heterocycle is twisted with respect with the metal coordination plane, the angles between the planes N1,C1,N2 and P1,Ni,C1,P2 being 60.1°. The Ni1–P1 and Ni1–P2 distances are identical, likewise the Ni1–N1 and Ni2–N2 separations of 2.825(4) and 2.828(4) Å, respectively, which are non-bonding, in contrast to Ni1–N2 in **8**. Consistently, the angles (heterocycle centroid)–C1–Ni and (heterocycle centroid)–Ni–H are 179.0(1)° and 170.2(1)°, respectively. The hydride ligand was located by Fourier difference (Ni1–H1 = 1.570 Å). Abstraction of the chloride ligand in **8** has generated a temporarily vacant coordination site at Ni that promoted the 1,2-migration of the H atom from C_{sp3} to Ni in **9**, thus completing the overall pyrimidinium C–H oxidative addition reaction to Ni^0 which converts **7** to **9**.

In agreement with the lack of observation of a hydrido, $N^{imine}C^{NHC}N^{imine}$ pincer complex in the reaction of Scheme 1, which contrasts with the relative stability of the hydrido complex **9**, attempts to abstract the chloride ligand from **2** with

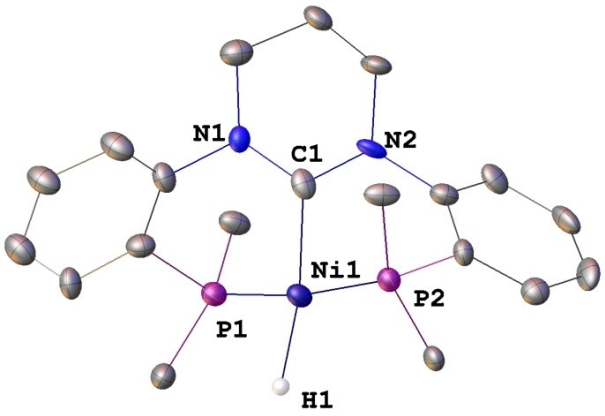

Figure 2. View of the structure of the cationic complex in [NiH($PC^{NHC}P$)]PF_6 (**9**) with H atoms omitted for clarity, except the Ni–H. Only the P-phenyl ipso carbons are shown. Thermal ellipsoids at the 50% probability level. Selected bond lengths (Å) and angles (deg): Ni1–C1 1.899(13), Ni1–P1 2.132(4), Ni1–P2 2.131(4), Ni1–H1 1.570; P1–Ni1–P2 171.43(15), C1–Ni–P1 85.0(4), C1–Ni–P2 86.7(4), C1–Ni1–H1 169.81, N1–C1–Ni1 121.3(9), N2–C1–Ni1 120.2(9), N1–C1–N2 118.5(11).

$TlPF_6$ in THF led to decomposition and no Ni–H signal was observed by in situ ^1H NMR monitoring. These results confirm the preference for $C_{sp3}{}^{H}$–Ni over C^{NHC}–Ni bonding in platforms of type **2**. Having established how the stepwise conversion of **7** to **9** occurs sheds light on the role of the anion associated with the azolium salt: a non-coordinating anion leads directly to carbene formation, as observed in Scheme 2, whereas a coordinating anion allows first the isolation of a complex with a $C_{sp3}{}^{H}$–Ni bond, as observed with **2** and **8**.

Theoretical calculations provided insights into the mechanism of formation of the hydrido complex **9** from **8**. We previously showed that H-migration in **2** from C_{sp3} to Ni to form a NHC donor was thermodynamically disfavoured owing to geometric constraints associated with a hypothetical $N^{imine}C^{NHC}N^{imine}$ pincer, which are relaxed in the $N^{imine}C_{sp3}{}^{H}N^{imine}$ system of **2**.[68] Starting from **8**, chloride abstraction leads to coordinatively unsaturated $\mathbf{8}_{I1}$ (Figure 3) from which H-migration to the cationic nickel centre affords a highly distorted tetrahedral $PC^{NHC}P$ intermediate $\mathbf{8}_{I2}$, with an associated barrier ($\mathbf{8}_{TS1}$) of 23.8 kcal mol^{-1}. A pathway leading from $\mathbf{8}_{I2}$ to the trans C^{NHC}–Ni–H product **9** would be associated with an energy barrier ($\mathbf{8}_{TS2}$, 33.4 kcal mol^{-1}), too high to be consistent with the experimental conditions and no other path has been found. However, the tetrahedral arrangement around Ni^{II} in $\mathbf{8}_{I2}$, typical of a triplet state, is more stable ($\Delta G = 16.4$ kcal mol^{-1}) than the computed singlet state ($\Delta G = 20.4$ kcal mol^{-1}). We then relaxed the structure of the triplet state $\mathbf{8}_{I2T}$ ($\Delta G = 16.3$ kcal mol^{-1}) from which H–migration in trans position becomes very easy ($\mathbf{8}_{TS2T}$, 18.7 kcal mol^{-1}) to give the triplet precursor $\mathbf{8}_{I3T}$ of **9**. It is noteworthy that $\mathbf{8}_{I3}$ ($\Delta G = +6.4$ kcal mol^{-1}), a singlet state intermediate retaining the conformation of the pincer in **8** (Figure 1), is less stable than the computed structure of **8**. The stabilisation of the hydride derivative **9** ($\Delta G = -4.3$ kcal mol^{-1}) results from a change in the conformation of the complex (Figure 4), made possible by the higher flexibility of the pincer ligand compared to that in **2**. According to our calculations, the formation of **9** is only possible because of the availability of this low-lying triplet state.

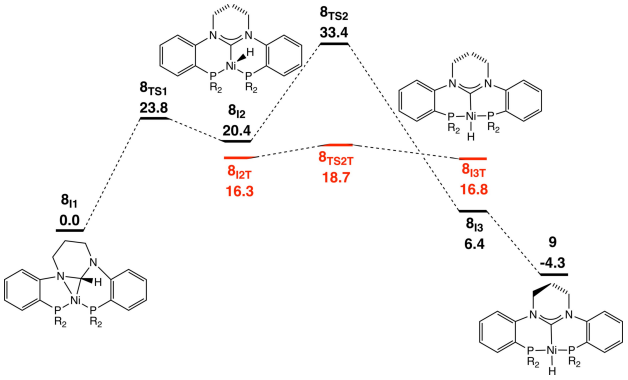

Figure 3. Mechanism for the formation of **9**. Energies are in kcal mol^{-1}. Values in black stand for the singlet potential energy surface (PES) and in red for the triplet PES. All H atoms except the migrating one are omitted for clarity.

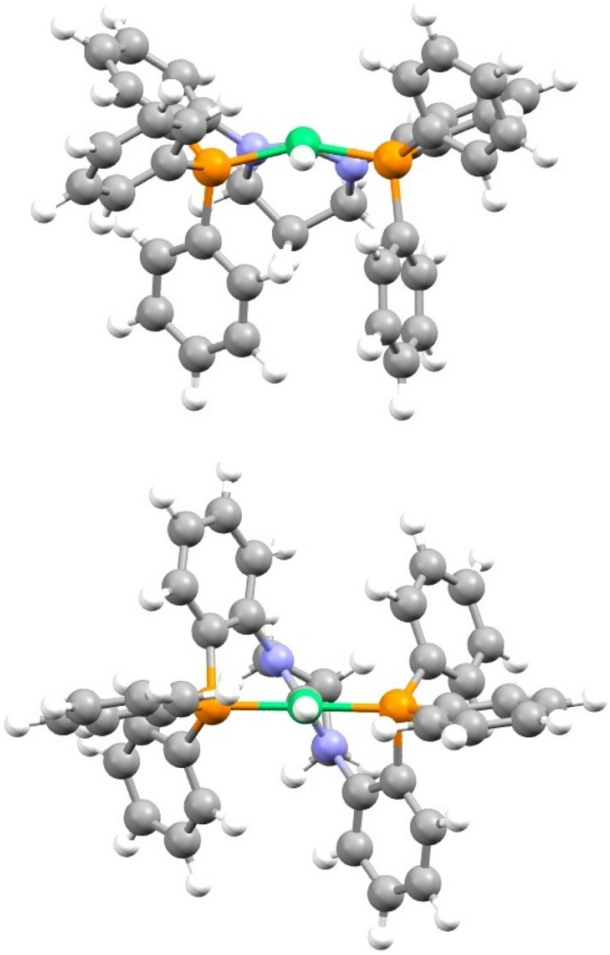

Figure 4. Views of the structures of $\mathbf{8}_{I3}$ (top) and **9** (bottom) along the C–Ni–H axis.

The subtle influence of the relative rigidity/flexibility of the pincer ligand is also apparent when comparing the (*o*-diphenylphosphino) aryl substituents with the more flexible (di-*t*-butylphosphaneyl) methyl groups, the former leading to an increased stability for the hydrido complex **9** (see Supporting Information, §1.15, Table S3 and Figure S30 for the crystal structure of $[NiF(P^{tBu}C^{NHC}P^{tBu})]PF_6$ (**18**)). Access to complex **9** prompted us to examine its reactivity towards ethylene. Nickel hydrido species play a central role in numerous catalytic reactions, such as the academically and industrially most relevant Ni-catalysed oligomerization of ethylene, but they are generally assumed rather than isolated.[50,52,56,70,74–79] Reaction of a THF solution of **9** with excess ethylene at room temperature afforded an orange solution from which single crystals of $\mathbf{10}\cdot 2(C_4H_8O)$ were obtained (Scheme 4). Their ^1H NMR spectrum showed the disappearance of the Ni–H resonance of **9** and contained new signals (a triplet and a quadruplet) corresponding to an ethyl group (see Supporting Information).

The structure of $[Ni(PC_{sp3}{}^{Et}P)]PF_6$ (**10**) in $\mathbf{10}\cdot 2(C_4H_8O)$ was determined by X-ray diffraction (Figures 5 and S24) and established that after ethylene insertion into the Ni–H bond,

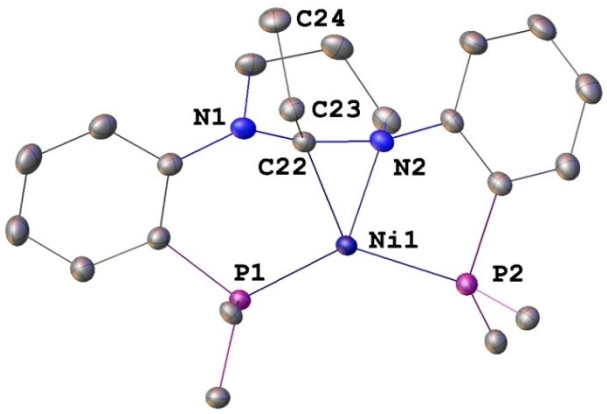

Figure 5. View of the structure of the cationic complex in $[Ni(PC^{Et}P)]PF_6$ (**10**·2(C_4H_8O)) with the solvent molecules and H atoms omitted for clarity. Only the P-phenyl ipso carbons are shown. Thermal ellipsoids at the 50% probability level. Selected bond lengths (Å) and angles (deg): Ni1–C22 1.8964(13), Ni1–N2 1.9289(11), Ni1–P1 2.1088(4), Ni1–P2 2.1673(4), N1–C22 1.424(2), N2–C22 1.441(2), C22–C23 1.519(2), C23–C24 1.533(2); P1–Ni1–P2 130.07(2), C22–Ni1–P1 93.70(4), C22–Ni1–P2 129.12(4), N2–Ni1–P1 137.28(4), N2–Ni1–P2 90.94(4), C22–Ni1–N2 44.24(5).

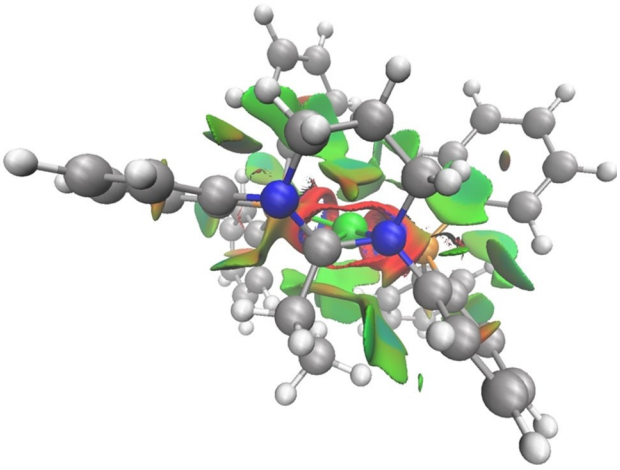

Figure 6. NCI analysis of **10**, in green area are attractive van der Waals forces and in red repulsive steric congestion.

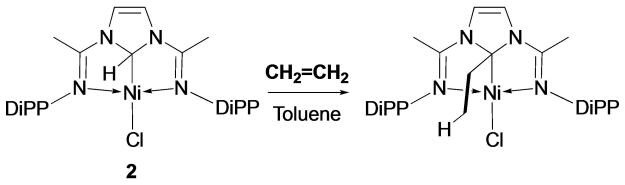

Scheme 5. Reaction of **2** with ethylene.[68]

the ethyl ligand has migrated to the $NC^{NHC}N$ carbene carbon to generate a C_{sp3}-hybridized carbon centre, with a typical C22–C23 single bond of 1.519(2) Å. The Ni1–C22 bond length of 1.8964(13) Å is shorter than the corresponding distance in **8** (1.942(1) Å), and the pyrimidine N2 atom is at a distance of 1.929(1) Å from the metal centre, which is also much shorter than that observed in the structure of **8** (2.531(1) Å). These features are possibly related to the electron donor character of the C22-bound ethyl group and consistently, the N2–C22 bond is longer than N1–C22 (1.441(2) and 1.424(2) Å, respectively). This cationic complex can thus be viewed as containing a pseudo-tricoordinate Ni^{II} centre with a C22–Ni σ-bond. This is supported by a NCI analysis, that shows the absence of *weak* interactions between the Ni cation and N2 or C22. Furthermore, the presence of a σ-hole along the Ni–N2 bond is typical of a dative bond (see Figure 6). When considering the midpoint M^{C-N} of the C22–N2 bond, the Ni–M^{C-N} distance is 1.772(2) Å and the M^{C-N}–Ni–P1 and M^{C-N}–Ni–P2 angles are 115.75(4) and 110.28(4)°, respectively.

Whereas ethyl migration from Ni to C^{NHC} was observed by Fryzuk and coll. when they reacted **4** with ethylene,[70,71] no formation of a Ni-ethyl group was observed when **2** was reacted with ethylene and "direct" insertion of ethylene into the C_{sp3}–H bond of **2** was envisaged, in agreement with theoretical calculations (Scheme 5).[68]

It is interesting to contrast the formation of the N-heterocyclic alkyl complex **10** with the Ni^0-catalyzed coupling reaction of simple azolium salts with ethylene affording C2-ethyl-substituted azolium salts where the C2 carbon remains sp^2-hybridized.[80] Clearly, the pincer nature of the ligand drastically alters the course of the reaction and we note that migration of a preformed benzyl ligand to a C^{NHC} has been reported in Zr^{IV} and Hf^{IV} $OC^{NHC}O$ pincer complexes,[43] which illustrates the broader relevance of such studies across the Periodic Table.

We are now in a position to perform comparative theoretical analyses on **2**, **4** and **9** and their respective ethylene insertion products to shed some light on the various steps involved in the reaction mechanism. The first obvious difference between these compounds is the presence of a hydrido ligand in **4** and **9**, contrary to **2**. For **4** and **9**, the mechanism of ethylene insertion is straightforward (Figure 7). After coordination (structure $\mathbf{9}_{I1}$), the ethylene molecule forms a C–H bond with the hydrido ligand, leading to $\mathbf{9}_{I2}$. In this structure, this newly formed C–H bond is elongated (1.180 Å) and the complex adopts a square based pyramidal structure, with the Ni

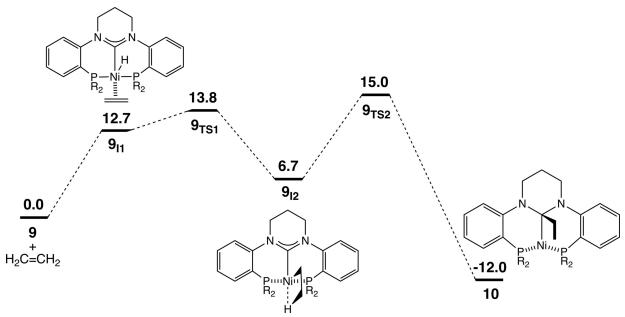

Figure 7. Mechanism for the ethylene insertion in **9**. Energies are in kcal mol^{-1}. All H atoms except the migrating one and those of the ethylene are omitted for clarity.

cation in the centre of the base. The resulting ethyl ligand is η^2-bound to the cationic metal centre through the H and C atoms. It can then directly migrate on the NHC donor carbon atom to form the carbanion. The associated transition state $\mathbf{9}_{TS2}$ is the rate determining step with a barrier of 15.0 kcal mol^{-1} so that the reaction is very easy. Consistent with the failed attempts to evidence/isolate a type **A** product (Scheme 4), no reaction path leading to **A** has been found and **A** would be less stable ($\Delta G = -7.5$ kcal mol^{-1}) than the thermodynamic product **10** ($\Delta G = -12.0$ kcal mol^{-1}).

For comparison, we computationally revisited the situation with **2** where the ethylene formally inserts in the C–H bond of the carbanion (Scheme 5). Attempts to find a direct insertion pathway failed and we were not able to coordinate the ethylene to the complex. This step is hampered by the rigidity of the tridentate pincer but decoordination of one of the imine donors is energetically accessible (Figure 8). The first step is thus a reorganisation of the Ni^{II} coordination sphere ($\mathbf{2}_{I1}$) followed by the transfer of the hydride to the ethylene ($\mathbf{2}_{I1}$ to $\mathbf{2}_{I3bis}$, Figure 8). This is followed by a second reorganisation of the Ni^{II} coordination sphere to place the ethyl ligand in cis position to the carbene ($\mathbf{2}_{I3bis}$ to $\mathbf{2}_{I4bis}$). This corresponds to the highest barrier found of 31.1 kcal mol^{-1} ($\mathbf{2}_{TS3}$), much higher than for **9**. The ethylation of the carbene carbon is then achieved in one step through $\mathbf{2}_{TS4}$. This is followed by the final recoordination of the imine donor to form $\mathbf{2}_{I6}$.

For both **4** and **9**, the mechanisms involve a hydride intermediate of which the stability allows a fast ethylene insertion in few steps with low energy barriers and without large geometric changes. In **2**, the hydrido complex being unstable, likewise for the coordination of the ethylene, the mechanism requires several drastic reorganisations of the Ni^{II} coordination sphere. This major difference can be attributed to the rigidity of the tridentate ligand in **2**.

We also examined the reactivity of **8** towards bases and its reaction with KHMDS in toluene afforded a major compound **11** that precipitated as dark red microcrystals from the reaction mixture owing to their poor solubility (Scheme 6). Its formation was accompanied by a minor product, which was subsequently obtained in higher yield using another protocol and identified as **15** by X-ray diffraction (see below). The disappearance of the ^{1}H NMR resonance assigned to the NiC_{sp3}–H proton of **8** indicated the formation of a carbene in **11**, which was confirmed by reaction of the latter with PPh_3 and CH_2Cl_2 (see below). Complex K[NiCl(PC^{NHC}P)] (**11**) was shown to be the potassium salt of an anionic, formally Ni^0 complex coordinated by a NHC, two phosphanes and a chloride (see Supporting Information). A related Ni^0 complex has been recently described, with 1-N-DiPP-benzimidoyl instead of phosphane pendant arms, and shown to activate ammonia,[64] which did not occur in our case. The electron-rich nature of the metal centre in the nickelate complex **11** explains its reaction with CH_2Cl_2 which yielded compound **12** containing a cationic, square planar Ni^{II} PC^{NHC}P pincer complex associated with a tetrahedral $[NiCl_4]^{2-}$ dianion (Supporting Information). An X-ray diffraction analysis confirmed its formulation as $[NiCl(PC^{NHC}P)]_2[NiCl_4]\cdot CH_2Cl_2$ (**12**$\cdot CH_2Cl_2$) (Figures 9 and S25). The bonding parameters in **12** are as expected for a NHC ligand coordinated to Ni^{II} and the twist of the heterocycle leads to an angle of 62.1° between the N1–C1–N2 plane and the mean metal coordination plane.

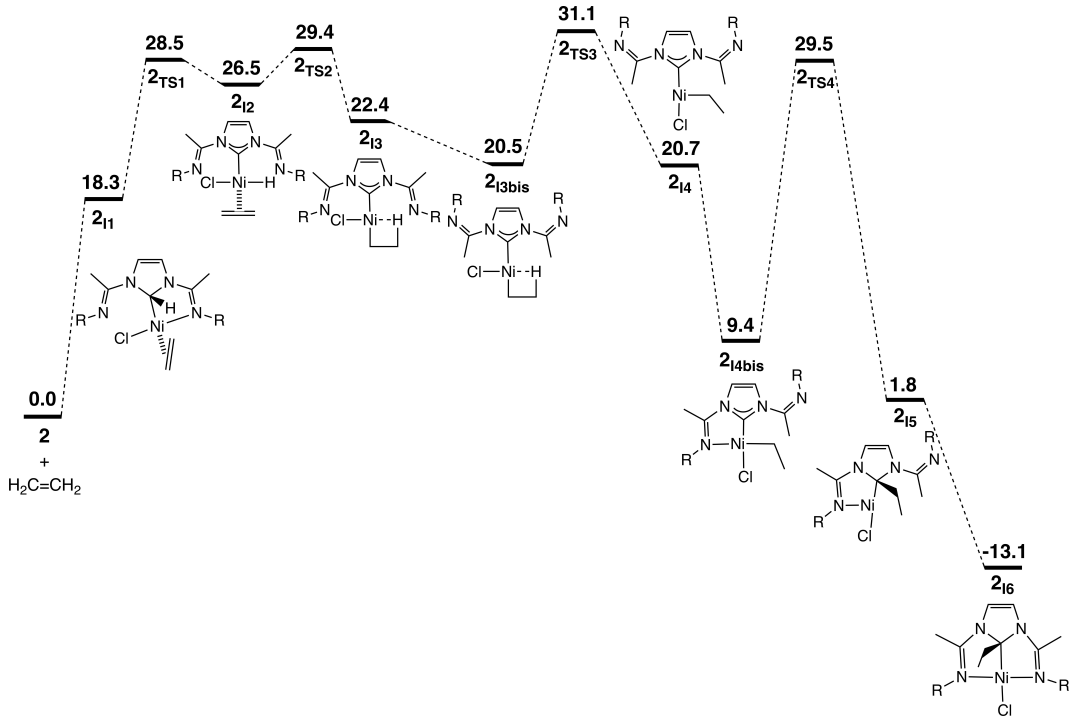

Figure 8. Mechanism for the ethylene insertion in **2**. Energies are in kcal mol^{-1}. All H atoms except the migrating one from $\mathbf{2}_{I1}$ to $\mathbf{2}_{I4}$ are omitted for clarity.

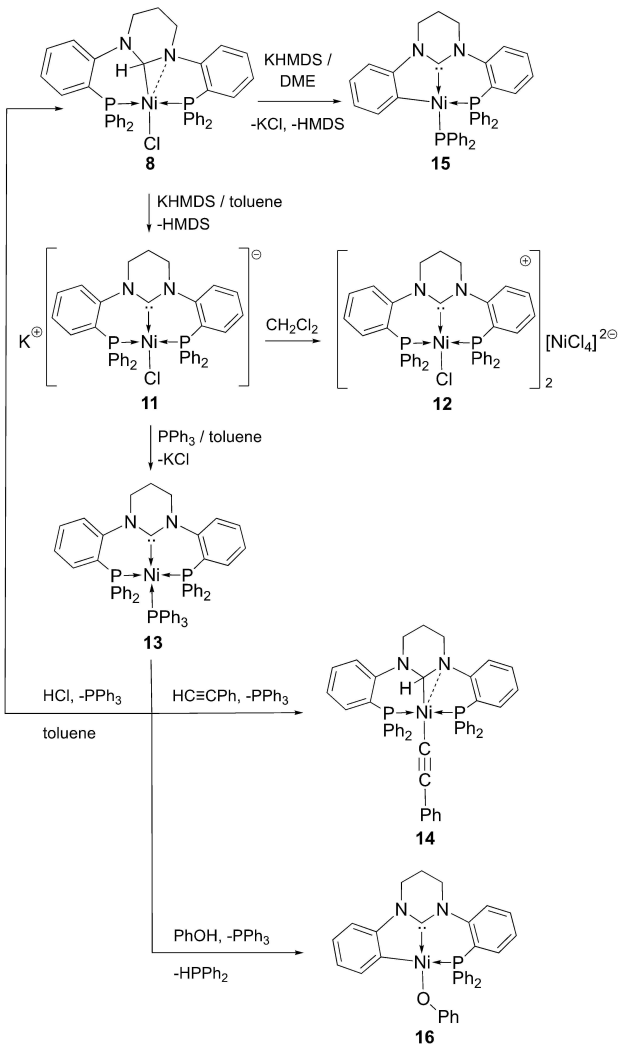

Scheme 6. P–C Bond activation in **8** affording the C–C^{NHC}–P pincer complex **15** with a terminal phophinido ligand; C–Cl bond activation by the Ni^0 complex **11** and reactions of **13** with acidic reagents.

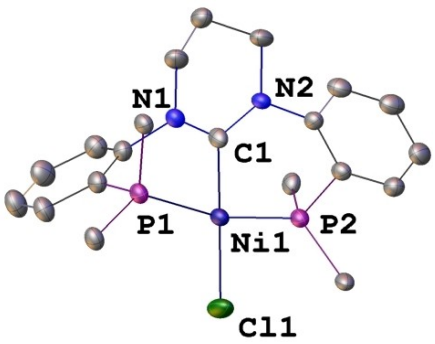

Figure 9. View of one molecule of the cationic complex of **12** in $[NiCl(PC^{NHC}P)]_2[NiCl_4]\cdot CH_2Cl_2$ (**12**·CH_2Cl_2) with H atoms omitted for clarity. The dianion $[NiCl_4]^{2-}$ and the solvent molecule are not shown. Only the P-phenyl ipso carbons are shown. Thermal ellipsoids at the 50% probability level. Selected bond lengths (Å) and angles (deg) in one of the molecules: Ni1–C1 1.911(4), Ni1–Cl1 2.1676(11), Ni1–P1 2.1854(11), Ni1–P2 2.1818(11), C1–N1 1.336(5), C1–N2 1.347(5); C1–Ni1–Cl1 176.64(12), P1–Ni1–P2 165.70(4), Ni1–C1–N1 120.4(3), Ni1–C1–N2 121.4(3).

Interestingly, the reaction of **11** with PPh_3 in toluene resulted in KCl precipitation and formation of a more soluble, neutral Ni^0 complex $[Ni(PC^{NHC}P)(PPh_3)]$ (**13**; Scheme 6). Its crystal structure established the distorted tetrahedral coordination environment of the metal, constituted by the $PC^{NHC}P$ pincer and a PPh_3 ligand (Figures 10 and S26). The bonding parameters are consistent with such a Ni^0 NHC complex.

It is noteworthy that the reaction of **13** with HCl afforded **8** in an oxidative addition-type process that transforms the NHC:→Ni unit into a C_{sp3}H–Ni–Cl moiety. Whether this occurs by oxidative addition of HCl at Ni^0 followed by H migration from Ni to C^{NHC} (the reverse of the conversion from **8** to **9**), or by "direct addition" across two centres, cannot be stated at this stage. Organic molecules with an acidic H also react with **13**, as shown with HC≡CPh which yielded the structurally characterized phenylacetylide complex $[Ni(C{\equiv}CPh)(PC_{sp3}{}^HP)]$ (**14**; Figures 11 and S27). Consistently, no reaction occurred between **13** and aniline. These reactions highlight the reactivity of the Ni^0–C^{NHC} moiety, and the ability of the $PC^{NHC}P$ pincer to stabilize both Ni^0 and Ni^{II} complexes while the $PC_{sp3}{}^HP$ pincer is only encountered in Ni^{II} chemistry. In **14**, the Ni1–C_{sp3} bond (1.960(2) Å) has a length similar to that in **8** and is trans to the Ni1–C_{sp} bond (Ni1–C41 = 1.890(3) Å). As was observed in complexes **8** and **10** containing a $PC_{sp3}{}^HP$ pincer, one of the heterocycle N atoms is closer to Ni than the other (Ni1–N1 = 2.576(2) and Ni1–N2 = 3.008(2) Å) but the Ni–N distances are much more similar to those in **8**. The N1–C1–N2 plane makes an angle of 81.1(1)° with the metal coordination plane.

When the reaction of **8** with KHMDS was performed in DME instead of toluene, the product was much more soluble and formation of **11** was not observed. Instead, HCl elimination

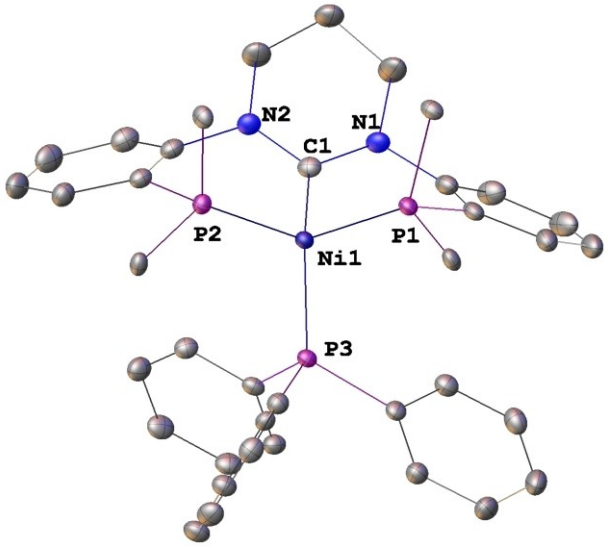

Figure 10. View of the structure of $[Ni(PC^{NHC}P)(PPh_3)]$ (**13**) with H atoms omitted for clarity. Only the P-phenyl ipso carbons of the pincer ligand are shown. Thermal ellipsoids at the 50% probability level. Selected bond lengths (Å) and angles (deg): Ni1–C1 1.9286(14), Ni1–P1 2.1379(4), Ni1–P2 2.1289(4), Ni1–P3 2.1624(4), N1–C1 1.375(2), N1–C2 1.381(2); C1–Ni1–P3 120.38(4), P1–Ni1–P2 117.61(2), P1–Ni1–P3 110.21(2), P2–Ni1–P3 113.75(2), N1–C1–Ni1 120.95(11), N2–C1–Ni1 123.82(10), N1–C1–N2 113.74(12).

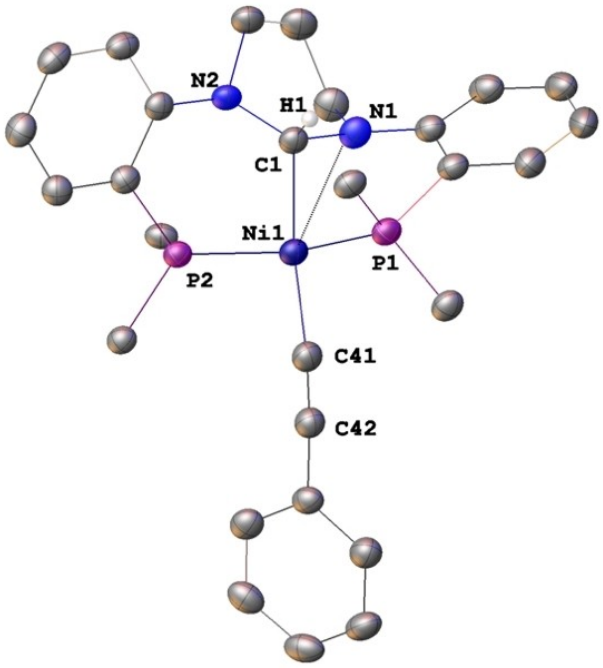

Figure 11. Structure of [Ni(C≡CPh)($PC_{sp3}^{H}P$)] (**14**) with H atoms omitted for clarity. Only the P-phenyl ipso carbons of the pincer ligand are shown. Thermal ellipsoids are shown at the 50% probability level. Selected bond lengths (Å) and angles (deg): Ni1–C1 1.960(2), Ni–N1 2.576, Ni1–P1 2.1649(7), Ni1–P2 2.1297(7), Ni1–C41 1.890(3), C41–C42 1.212(4), N1–C1 1.463(3), N2–C1 1.481(3); N1–C1–Ni1 96.54(15), N2–C1–Ni1 121.27(16), C1–Ni1–C41 163.96(11), P1–Ni1–P2 155.76(3), Ni1–C41–C42 173.2(2).

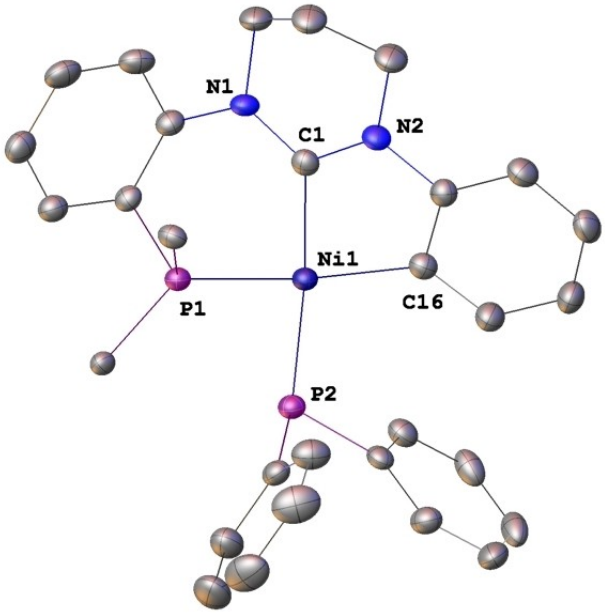

Figure 12. View of the structure of [Ni(PPh_2)($CC^{NHC}P$)] (**15**) with H atoms omitted for clarity. Only the ipso carbons of the phenyls at P1 are shown. Thermal ellipsoids are shown at the 50% probability level. Ni1–C1 1.934(2), Ni1–C16 1.935(2), Ni1–P1 2.2019(5), Ni1–P2 2.2178(5), C1–N1 1.356(2), C1–N2 1.344(2); C1–Ni1–P2 170.79(6), C1–Ni1–C16 83.27(8), C1–Ni1–P1 85.84(6), C16–Ni1–P1 156.71(6), P1–Ni1–P2 91.58(2), N1–C1–Ni1 130.3(1), N2–C1–Ni1 112.7(1).

resulted in carbene formation and a remarkable intramolecular rearrangement yielded [Ni(PPh_2)($CC^{NHC}P$)] (**15**) with a Ni^{II} centre in a square planar coordination environment, as established by X-ray diffraction (Figures 12 and S28). Thus, following C–P bond activation, a PPh_2 group has migrated from the pincer ligand to the metal to give a still rare example of terminal phosphanido ligand on Ni, with concomitant formation of a direct C_{aryl}–Ni covalent bond. To the best of our knowledge, this rearrangement is unprecedented in pincer chemistry. We suggest that it occurs via a formally tricoordinate, reactive Ni^0 species where the metal inserts into a pincer C–P bond (see Scheme S1 in the Supporting Information). The ^{31}P NMR singlet of **8** at δ 4.0 is replaced in [Ni(PPh_2)($CC^{NHC}P$)] (**15**) by an AB pattern at δ = 48.32 and 16.68 (^2J(P–P) = 30.1 Hz) for the phosphanido and phosphane ligands, respectively. The chemical shift of the former resonance is consistent with values reported very recently for Ni^{II} complexes containing terminal diphenylphosphanido ligands.[81] The Ni1–C1 and Ni1–C16 bond lengths of 1.934(2) and 1.935(2) Å are consistent with C_{sp2}-hybridized carbon atoms. The Ni1–P2 bond length of 2.2178(5) Å indicates a terminal phosphanido ligand in trans position to a ligand with a strong trans-influence.[81] The Ni1–P1 bond length of 2.2019(5) Å is also indicative of the trans influence of the aryl ligand at C16. It is interesting to recall that reactions related to a "reverse" of the P–C bond breaking reaction leading to **15** were observed (i) in Ni^{II} phosphinite/phosphane complexes,[82] (ii) when metallacyclic Pd^{II} complexes containing C,P and P,O chelates were reacted with $PPhCl_2$ with formation of C–P and O–P bonds,[83,84] and in Pt cluster chemistry with the reductive coupling of a bridging μ-PPh_2 group with a *cis*-phenyl ligand to form a PPh_3 ligand.[85] Note, however, that in cases (i) and (ii), the PR_2 group does not originate from a phosphanido ligand.

In toluene, **11** is likely present as a tight ion-pair, where the potassium cation is possibly close to the chloride ligand, which prevents the rearrangement leading to **15**. However, upon dissolution of **11** in THF or DME, KCl precipitated, generating a transient reactive Ni^0 species and rapid formation of **15** was observed. Furthermore, monitoring a solution of pure **13** by ^{31}P NMR in benzene or THF showed that partial dissociation of PPh_3 occurred with concomitant formation of **15**, which supports the involvement in both cases of a formally tricoordinate, reactive Ni^0 species as intermediate. This hypothesis is supported by the computed mechanism. We modelled the evolution of **8** in toluene and in DME after its reaction with KHMDS. In both cases, a neutral Ni^0 complex **8N** was obtained, weakly interacting with KCl through the potassium and not the chlorine. A key difference is that the departure of KCl from **8N** is exergonic in DME and endergonic in toluene. The subsequent Ni^0 insertion into the C–P bond is associated with very low energy barriers for $\mathbf{8N_{TS1}}$ in both solvents: ΔG = 13.3 and 16.1 kcal mol^{-1} in DME and toluene, respectively (Figure 13). Such low and similar barriers cannot explain the difference in reactivity, and it is most likely the low solubility of KCl in toluene that prevents its dissociation and thus inhibits the reaction.

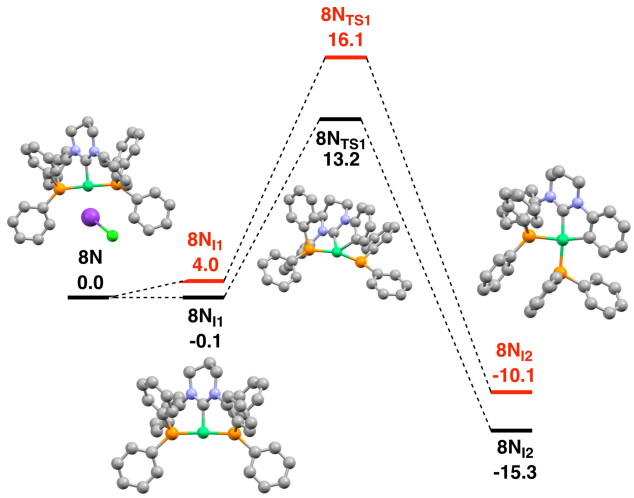

Figure 13. Mechanism for the intramolecular P–C oxidative addition in **8N** leading to **15**, in red are the values in toluene and in black in DME. Energies are in kcal mol^{-1}.

Furthermore, **13** reacted with phenol (p*Ka* = 10), another compound with an acidic proton, to afford **16**, which was characterized by X-ray diffraction as a phenoxy derivative in which P–C bond activation of the pincer has occurred, like in **15** (Scheme 6 and Figures 14 and S29). It is reasonable to assume that the phenol assisted the displacement of PPh_3 from **13**, favouring the formation of **15** which reacted with PhOH to eliminate the phosphanido ligand as $HPPh_2$ and give [Ni(OPh)(CC^{NHC}P)] (**16**). This was verified by a NMR experiment where a benzene solution of pure [Ni(PPh_2)(CC^{NHC}P)] (**15**) was reacted with phenol and rapid and quantitative formation of [Ni(OPh)(CC^{NHC}P)] (**16**) was observed. In contrast, upon addition of methanol (p*Ka* = 15.5) to **13**, no O–H bond activation occurred, and only reversible coordination of the alcohol was observed by ^{1}H NMR spectroscopy, consistent with its lower acidity. The structure of **16** is similar to that of **15**, with the Ni centre in a slightly distorted square planar environment and a phenoxy ligand replacing the phosphanido ligand. Its bending (Ni1–O1–C29 129.8(1)°) is consistent with an essentially σ-bonding interaction with the metal centre. There is a slight tilt of the NHC ligand, which results in different Ni1–N1 and Ni1–N2 distances of 2.741(1) and 2.959(1) Å, respectively. The other metrical data are comparable with those of other complexes described in this work.

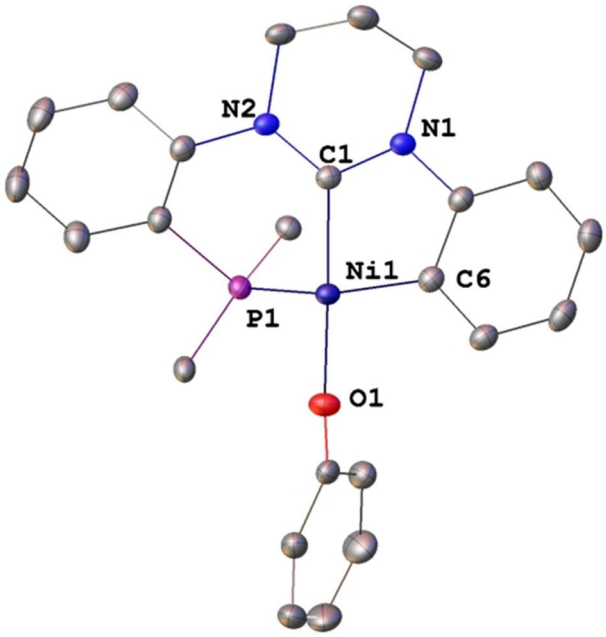

Figure 14. View of the structure of [Ni(OPh)(CC^{NHC}P)] (**16**) with H atoms omitted for clarity. Only the *ipso* carbons of the phenyls at P1 are shown. Thermal ellipsoids at the 50% probability level. Selected bond lengths (Å) and angles (deg): Ni1–C1 1.9036(14), Ni1–C6 1.8975(15), Ni1–P1 2.2242(4), Ni1–O1 1.876(1), N1–C1 1.348(2), N2–C1 1.357(2); C1–Ni1–O1 165.65(5), C1–Ni1–C6 83.18(6), C1–Ni1–P1 85.94(4), P1–Ni1–C6 154.12(5), O1–Ni1–C6 91.52(6), O1–Ni1–P1 104.02(4), Ni1–O1–C29 129.8(1), N1–C1–Ni1 113.8(1), N2–C1–Ni1 129.5(1).

These C–P bond activation and C–Ni and P–Ni bond forming reactions were initially promoted by the liberation of a coordination site at Ni in **8** resulting from HCl elimination and formation of a tricoordinate, Ni^0 intermediate (Scheme S1 in Supporting Information). Accordingly, and as shown with the isolation of **13**, addition of a neutral donor ligand, like PPh_3, that can occupy this vacant coordination site, prevents this process, which can be described as an intramolecular Ni^0 insertion into the C_{aryl}–P bond. Having now characterized **15**, we could identify that it was the minor product detected by ^{31}P NMR in the reaction of **8** with KHMDS in toluene, which afforded **11** as the major product. The poor solubility of **11** in toluene hampered its subsequent transformation, in contrast to the situation in DME, and this emphasizes the critical role of the solvent in such reactions.

Conclusion

It was found that combining in a Ni-coordinated pincer ligand a bridgehead NHC donor from a flexible six-membered pyrimidine-type heterocycle with rigid phosphane donors as side arms results in a number of unique features. First, reaction of the proligand azolium C_{sp2}–H bond by [Ni(cod)$_2$] leads to its reduction and generates a carbanionic ligand (with a Ni–C_{sp3} bond) in [NiCl(PC$_{sp3}^{H}$P)] (**8**) rather than the expected carbene donor (with a C^{NHC}–Ni bond). Subsequent halide abstraction from **8** generates a vacant coordination site at the metal that triggers its transformation in the NHC, hydrido complex [NiH(PC^{NHC}P)]PF_6 (**9**). If ethylene inserts into the Ni–H bond of the latter complex, no Ni–Et complex was observed because of rapid ethyl migration with C–C bond formation involving the N–*C*–N carbon of the heterocycle, as was evidenced with the characterization of [Ni(PC^{Et}P)]PF_6 (**10**). Our results underline the subtle balance of electronic and steric effects in C–H bond-activation and C–C bond-formation processes that are central to reactivity and catalytic studies and allow to better understand and rationalize previous results on related systems. Finally, an unprecedented C–P bond activation reaction result-

ing in the transformation of the P–C^{NHC}–P pincer of **8** in a C–C^{NHC}–P pincer with formation of a Ni^{II} complex with a terminal phosphanido ligand in [Ni(PPh_2)($CC^{NHC}P$)] (**15**) is not only of fundamental interest but also shows that the thermodynamic stability brought about by a pincer platform does not preclude its reactivity and transformation in a different and unexpected pincer system. This can serve as a *caveat* in further studies with phosphane-containing pincer ligands. That all these bond forming/breaking reactions were found to readily occur in the coordination sphere of a Ni centre highlights the versatility of this metal, consistent with its central role in catalytic transformations. Theoretical calculations allowed to rationalize the experimental observations and suggested the sequence of elementary steps involved, which open new perspectives and provide guiding tools for further developments.

Deposition Numbers 2116366 (**8**·C_6H_6), 2116367 (**9**), 2116368 (**10**·2(C_4H_8O)), 2116369 (**12**·CH_2Cl_2), 2116370 (**13**), 2116371 (**14**), 2116372 (**15**), 2116373 (**16**) and 2116374 (**18**) contain the supplementary crystallographic data for this paper. These data are provided free of charge by the joint Cambridge Crystallographic Data Centre and Fachinformationszentrum Karlsruhe Access Structures service.

Acknowledgements

We are very grateful to the School of Chemistry and Chemical Engineering, Yangzhou University, Jiangsu, P. R. China for a postdoctoral grant to F.H. and to the China Postdoctoral Science Foundation (Grant No. 2019M651975) for funding, and the CNRS and the MESRI (Paris) for support. We thank Drs. L. Karmazin, C. Bailly and Dr. N. Gruber (Service de Radiocristallographie, Fédération de Chimie Le Bel, FR2010, Université de Strasbourg/CNRS) for the determination of the crystal structures, and the Computation Centre of Strasbourg for computing time.

Conflict of Interest

The authors declare no conflict of interest.

Data Availability Statement

The data that support the findings of this study are available from the corresponding author upon reasonable request.

Keywords: C–H bond activation · C–P bond activation · ethylene insertion · N-heterocyclic carbenes · pincer ligands

[1] T. P. Nicholls, J. R. Williams, C. E. Willans, in *Adv. Organomet. Chem., Vol. 75* (Ed.: P. J. Pérez), Academic Press, **2021**, pp. 245–329.
[2] S. C. Sau, P. K. Hota, S. K. Mandal, M. Soleilhavoup, G. Bertrand, *Chem. Soc. Rev.* **2020**, *49*, 1233–1252.
[3] R. J. Rama, M. T. Martín, R. Peloso, M. C. Nicasio, in *Adv. Organomet. Chem., Vol. 74* (Ed.: P. J. Pérez), Academic Press, **2020**, pp. 241–323.
[4] A. A. Danopoulos, T. Simler, P. Braunstein, *Chem. Rev.* **2019**, *119*, 3730–3961.
[5] S. Shi, S. P. Nolan, M. Szostak, *Acc. Chem. Res.* **2018**, *51*, 2589–2599.
[6] H. V. Huynh, *Chem. Rev.* **2018**, *118*, 9457.
[7] H. V. Huynh, *The Organometallic Chemistry of N-Heterocyclic Carbenes*, John Wiley & Sons Ltd, **2017**.
[8] M. N. Hopkinson, C. Richter, M. Schedler, F. Glorius, *Nature* **2014**, *510*, 485–496.
[9] K. Riener, S. Haslinger, A. Raba, M. P. Högerl, M. Cokoja, W. A. Herrmann, F. E. Kühn, *Chem. Rev.* **2014**, *114*, 5215–5272.
[10] R. H. Crabtree, *Coord. Chem. Rev.* **2013**, *257*, 755–766.
[11] D. J. Nelson, S. P. Nolan, *Chem. Soc. Rev.* **2013**, *42*, 6723–6753.
[12] S. Díez-González, N. Marion, S. P. Nolan, *Chem. Rev.* **2009**, *109*, 3612–3676.
[13] O. Schuster, L. Yang, H. G. Raubenheimer, M. Albrecht, *Chem. Rev.* **2009**, *109*, 3445–3478.
[14] F. E. Hahn, M. Jahnke, *Angew. Chem. Int. Ed.* **2008**, *47*, 3122–3172.
[15] S. Wuertz, F. Glorius, *Acc. Chem. Res.* **2008**, *41*, 1523.
[16] F. Glorius, *N-Heterocyclic Carbenes in Transition Metal Catalysis*, Springer Berlin Heidelberg, Berlin, Heidelberg, **2007**.
[17] W. A. Herrmann, *Angew. Chem. Int. Ed.* **2002**, *41*, 1290–1309.
[18] W. A. Herrmann, M. Elison, J. Fischer, C. Köcher, G. R. Artus, *Angew. Chem. Int. Ed. Engl.* **1995**, *34*, 2371–2374.
[19] F. E. Hahn, *Chem. Rev.* **2018**, *118*, 9455–9456.
[20] R. Jordan, D. Kunz, *Molecules* **2021**, *26*.
[21] Y. D. Wang, B. Zhang, S. Guo, *Eur. J. Inorg. Chem.* **2021**, *2021*, 188–204.
[22] N. U. D. Reshi, J. K. Bera, *Coord. Chem. Rev.* **2020**, 213334.
[23] R. Taakili, Y. Canac, *Molecules* **2020**, *25*.
[24] C. V. Thompson, Z. J. Tonzetich, in *Adv. Organomet. Chem., Vol. 74* (Ed.: P. J. Pérez), Academic Press, **2020**, pp. 153–240.
[25] T. Toda, S. Kuwata, *J. Organomet. Chem.* **2020**, *917*, 121270.
[26] K. Junge, V. Papa, M. Beller, *Chem. Eur. J.* **2019**, *25*, 122–143.
[27] S. M. Rummelt, J. M. Darmon, R. P. Yu, P. Viereck, T. P. Pabst, Z. R. Turner, G. W. Margulieux, S. L. Gu, P. J. Chirik, *Organometallics* **2019**, *38*, 3159–3168.
[28] H. Valdés, E. Rufino-Felipe, D. Morales-Morales, *J. Organomet. Chem.* **2019**, *898*, 120864.
[29] X. Ren, M. Wesolek, P. Braunstein, *Dalton Trans.* **2019**, *48*, 12895–12909.
[30] J. Cheng, L. Wang, P. Wang, L. Deng, *Chem. Rev.* **2018**, *118*, 9930–9987.
[31] H. Valdés, M. A. García-Eleno, D. Canseco-Gonzalez, D. Morales-Morales, *ChemCatChem* **2018**, *10*, 3136–3172.
[32] M. M. Gan, J. Q. Liu, L. Zhan, Y. Y. Wang, F. E. Hahn, Y. F. Han, *Chem. Rev.* **2018**, *118*, 9587–9641.
[33] L. González-Sebastián, A. B. Chaplin, *Inorg. Chim. Acta* **2017**, *460*, 22–28.
[34] C. F. Harris, M. B. Bayless, N. P. van Leest, Q. J. Bruch, B. N. Livesay, J. Bacsa, K. I. Hardcastle, M. P. Shores, B. de Bruin, J. D. Soper, *Inorg. Chem.* **2017**, *56*, 12421–12435.
[35] V. Charra, P. de Frémont, P. Braunstein, *Coord. Chem. Rev.* **2017**, *341*, 53–176.
[36] S. Hameury, P. de Frémont, P. Braunstein, *Chem. Soc. Rev.* **2017**, *46*, 632–733.
[37] M. Martín, E. Sola, in *Adv. Organomet. Chem., Vol. 73* (Ed.: P. J. Pérez), Academic Press, **2020**, pp. 79–193.
[38] H. F. Li, T. P. Goncalves, D. Lupp, K. W. Huang, *ACS Catal.* **2019**, *9*, 1619–1629.
[39] D. Morales-Morales, *Pincer Compounds – Chemistry and Applications*, Elsevier, **2018**.
[40] E. Peris, R. H. Crabtree, *Chem. Soc. Rev.* **2018**, *47*, 1959–1968.
[41] J. Sun, L. Luo, Y. Luo, L. Deng, *Angew. Chem. Int. Ed.* **2017**, *56*, 2720–2724.
[42] R. S. Ramón, S. P. Nolan, A. Börner, R. Jackstell, F. Hapiot, E. Monflier, M. Schwarze, R. Schomäcker, D. E. Bergbreiter, L. T. Pilarski, K. J. Szabó, R. Kourist, U. T. Bornscheuer, *Applied Homogeneous Catalysis with Organometallic Compounds* **2017**, 809–950.
[43] C. Romain, D. Specklin, K. Miqueu, J.-M. Sotiropoulos, C. Fliedel, S. Bellemin-Laponnaz, S. Dagorne, *Organometallics* **2015**, *34*, 4854–4863.
[44] C. Fliedel, P. Braunstein, *J. Organomet. Chem.* **2014**, *751*, 286–300.
[45] G. van Koten, D. Milstein, *Organometallic Pincer Chemistry*, Springer, Berlin, Heidelberg, **2013**.
[46] S. Gaillard, J. L. Renaud, *Dalton Trans.* **2013**, *42*, 7255–7270.
[47] D. Pugh, A. A. Danopoulos, *Coord. Chem. Rev.* **2007**, *251*, 610–641.
[48] K. Fischer, K. Jonas, P. Misbach, R. Stabba, G. Wilke, *Angew. Chem. Int. Ed.* **1973**, *12*, 943–953.

[49] P. W. Jolly, *The Organic Chemistry of Nickel*, Academic Press, **1974**.
[50] W. Keim, *Angew. Chem. Int. Ed.* **1990**, *29*, 235–244.
[51] D. Zargarian, *Nickel: Organometallic Chemistry, in Encyclopedia of Inorganic and Bioinorganic Chemistry*, John Wiley & Sons, **2011**.
[52] W. Keim, *Angew. Chem. Int. Ed.* **2013**, *52*, 12492–12496.
[53] A. Prakasham, P. Ghosh, *Inorg. Chim. Acta* **2015**, *431*, 61.
[54] D. M. Flanigan, F. Romanov-Michailidis, N. A. White, T. Rovis, *Chem. Rev.* **2015**, *115*, 9307–9387.
[55] W. A. Herrmann, B. Cornils, R. S. Ramón, S. P. Nolan, A. Börner, R. Jackstell, F. Hapiot, E. Monflier, M. Schwarze, R. Schomäcker, D. E. Bergbreiter, L. T. Pilarski, K. J. Szabó, R. Kourist, U. T. Bornscheuer, *Applied Homogeneous Catalysis with Organometallic Compounds* **2017**, 1–22.
[56] H. Olivier-Bourbigou, P. A. R. Breuil, L. Magna, T. Michel, M. F. Espada Pastor, D. Delcroix, *Chem. Rev.* **2020**, *120*, 7919–7983.
[57] S. Gu, J. Du, J. Huang, Y. Guo, L. Yang, W. Xu, W. Chen, *Dalton Trans.* **2017**, *46*, 586–594.
[58] F. Zhang, X. M. Cao, J. W. Wang, J. J. Jiao, Y. M. Huang, M. Shi, P. Braunstein, J. Zhang, *Chem. Commun.* **2018**, *54*, 5736–5739.
[59] E. L. Kolychev, I. A. Portnyagin, V. V. Shuntikov, V. N. Khrustalev, M. S. Nechaev, *J. Organomet. Chem.* **2009**, *694*, 2454.
[60] A. M. Magill, K. J. Cavell, B. F. Yates, *J. Am. Chem. Soc.* **2004**, *126*, 8717–8724.
[61] R. Alder, M. E. Blake, J. M. Oliva, *J. Phys. Chem. A* **1999**, *103*, 11200–11211.
[62] M. Cybularczyk-Cecotka, A. M. Dąbrowska, P. A. Guńka, P. Horeglad, *Inorganics* **2018**, *6*.
[63] T. Wurm, F. Mulks, C. R. N. Böhling, D. Riedel, P. Zargaran, M. Rudolph, F. Rominger, A. S. K. Hashmi, *Organometallics* **2016**, *35*, 1070–1078.
[64] R. M. Brown, J. Borau Garcia, J. Valjus, C. J. Roberts, H. M. Tuononen, M. Parvez, R. Roesler, *Angew. Chem. Int. Ed.* **2015**, *54*, 6274–6277.
[65] L. B. Delvos, A. Hensel, M. Oestreich, *Synthesis* **2014**, *46*, 2957–2964.
[66] L. Schwartsburd, M. F. Mahon, R. C. Poulten, M. R. Warren, M. K. Whittlesey, *Organometallics* **2014**, *33*, 6165–6170.
[67] J. J. Dunsford, K. J. Cavell, *Organometallics* **2014**, *33*, 2902–2905.
[68] X. Ren, C. Gourlaouen, M. Wesolek, P. Braunstein, *Angew. Chem. Int. Ed.* **2017**, *56*, 12557–12560.
[69] D. S. McGuinness, K. J. Cavell, B. F. Yates, B. W. Skelton, A. H. White, *J. Am. Chem. Soc.* **2001**, *123*, 8317–8328.
[70] T. Steinke, B. K. Shaw, H. Jong, B. O. Patrick, M. D. Fryzuk, *Organometallics* **2009**, *28*, 2830–2836.
[71] T. Steinke, B. K. Shaw, H. Jong, B. O. Patrick, M. D. Fryzuk, J. C. Green, *J. Am. Chem. Soc.* **2009**, *131*, 10461–10466.
[72] B. F. Pan, S. Pierre, M. W. Bezpalko, J. W. Napoline, B. M. Foxman, C. M. Thomas, *Organometallics* **2013**, *32*, 704–710.
[73] V. Subramaniyan, B. Dutta, A. Govindaraj, G. Mani, *Dalton Trans.* **2019**, *48*, 7203–7210.
[74] a) W. Keim, F. H. Kowaldt, R. Goddard, C. Krüger, *Angew. Chem. Int. Ed. Engl.* **1978**, *17*, 466–467; b) M. Peuckert, W. Keim, *Organometallics* **1983**, *2*, 594–597; c) W. Keim, A. Behr, B. Gruber, B. Hoffmann, F. H. Kowaldt, U. Kuerschner, B. Limbaecker, F. P. Sistig, *Organometallics* **1986**, *5*, 2356–2359.
[75] U. Müller, W. Keim, C. Krüger, P. Betz, *Angew. Chem. Int. Ed. Engl.* **1989**, *28*, 1011–1013.
[76] P. Braunstein, Y. Chauvin, S. Mercier, L. Saussine, A. DeCian, J. Fischer, *J. Chem. Soc. Chem. Commun.* **1994**, 2203–2204.
[77] E. M. Matson, G. Espinosa Martinez, A. D. Ibrahim, B. J. Jackson, J. A. Bertke, A. R. Fout, *Organometallics* **2015**, *34*, 399–407.
[78] Z. J. Wang, X. Y. Li, H. J. Sun, O. Fuhr, D. Fenske, *Organometallics* **2018**, *37*, 539–544.
[79] R. Das, J. Blumenberg, C. G. Daniliuc, D. Schnieders, J. Neugebauer, Y.-F. Han, F. E. Hahn, *Organometallics* **2019**, *38*, 3278–3285.
[80] A. T. Normand, K. J. Hawkest, N. D. Clernentt, K. J. Cavell, B. F. Yates, *Organometallics* **2007**, *26*, 5352–5363.
[81] S. Sabater, D. Schmidt, H. Schmidt, M. W. Kuntze-Fechner, T. Zell, C. J. Isaac, N. A. Rajabi, H. Grieve, W. J. M. Blackaby, J. P. Lowe, S. A. Macgregor, M. F. Mahon, U. Radius, M. K. Whittlesey, *Chem. Eur. J.* **2021**, *27*, 13221–13234.
[82] L. P. Mangin, D. Zargarian, *Organometallics* **2019**, *38*, 4687–4700.
[83] P. Braunstein, D. Matt, D. Nobel, J. Fischer, *J. Chem. Soc. Chem. Commun.* **1987**, 1530–1532.
[84] F. Balegroune, P. Braunstein, D. Grandjean, D. Matt, D. Nobel, *Inorg. Chem.* **1988**, *27*, 3320–3325.
[85] a) C. Archambault, R. Bender, P. Braunstein, A. De Cian, J. Fischer, *J. Chem. Soc. Chem. Commun.* 1996, 2729–2730; b) R. Bender, R. Welter, P. Braunstein, *Inorg. Chim. Acta* **2015**, *424*, 20–28.

Manuscript received: November 26, 2021
Accepted manuscript online: January 5, 2022
Version of record online: January 27, 2022